

pubs.acs.org/est Article

Size and Strain of Zinc Sulfide Nanoparticles Altered by Interaction with Organic Molecules

Maureen Le Bars,* Clément Levard, Samuel Legros, Vladimir Vidal, Alejandro Fernandez-Martinez, F. Marc Michel, Antoine Thill, Benedicte Prelot, Gabrielle Dublet-Adli, Daniel Borschneck, Jérôme Rose, and Emmanuel Doelsch



Cite This: Environ. Sci. Technol. 2022, 56, 16831–16837



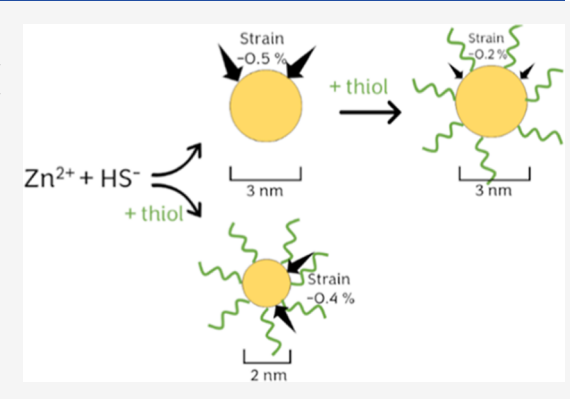
ACCESS

Metrics & More

Article Recommendations

Supporting Information

ABSTRACT: Nanosized zinc sulfides (nano-ZnS) have size-dependent and tunable physical and chemical properties that make them useful for a variety of technological applications. For example, structural changes, especially caused by strain, are pronounced in nano-ZnS < 5 nm in size, the size range typical of incidental nano-ZnS that form in the environment. Previous research has shown how natural organic matter impacts the physical properties of nano-ZnS but was mostly focused on their aggregation state. However, the specific organic molecules and the type of functional groups that are most important for controlling the nano-ZnS size and strain remain unclear. This study examined the size-dependent strain of nano-ZnS synthesized in the presence of serine, cysteine, glutathione, histidine, and acetate. Synchrotron total scattering pair distribution function analysis was used to determine the average crystallite size and strain. Among the different



organic molecules tested, those containing a thiol group were shown to affect the particle size and size-induced strain most strongly when added during synthesis but significantly reduced the particle strain when added to as-formed nano-ZnS. The same effects are useful to understand the properties and behavior of natural nano-ZnS formed as products of microbial activity, for example, in reducing environments, or of incidental nano-ZnS formed in organic wastes.

KEYWORDS: thiol, pair distribution function, sphalerite, lattice contraction, structure, ZnS

1. INTRODUCTION

Zinc sulfide nanoparticles (nano-ZnS) are of great interest due to their size-dependent electric and optical properties that can be tuned for different technological applications. 1,2 Nano-ZnS can also be found in nature, for example, in systems undergoing sulfate reduction by bacteria^{3,4} or formed incidentally in liquid and anaerobically digested zinc-rich organic waste (OW) used as the agricultural fertilizer. Nano-ZnS formed in OW are 3-5 nm in size and have been shown to undergo transformation in days or months in OW or amended soils. 5,7,9 Considering the high concentration of Zn in OW combined with the amount of OW applied on croplands, we previously estimated that 440,000 tons of nano-ZnS are released into the environment each year. 10 Sulfur in soil is an essential macronutrient for plants, 11 and its reduction to sulfide can lead to the immobilization of chalcophile metals (Fe, Cu, Cd, Hg) through metal sulfide precipitation. 12 Zinc also plays a crucial role in human functioning and in plant proteins. However, millions of hectares of cropland suffer from Zn deficiency. 15-17 On the other hand, Zn can be toxic for plants, 18 and Zn toxicity in crops can occur in contaminated soils, for example, in agricultural soils treated with sewage sludge. 19 Considering the high volume of nano-ZnS spread on

soils, understanding their formation and transformation is crucial to be able to predict zinc and sulfur cycling.

Studies of synthetic nano-ZnS have shown that the particle size has a significant impact on their chemical properties and structure. For example, Zhang et al. $(2010)^{20}$ showed that the total free surface energy of nano-ZnS was size-dependent at sizes ranging from 2 to 6 nm, which affected their dissolution rate in an EDTA-containing medium. Gilbert et al. $(2004)^{21}$ reported that 3.4 nm ZnS undergoes significant structural strain, as indicated by an average of 1% lattice contraction compared to that in bulk ZnS. Indeed, Jiang et al. $(2001)^{22}$ demonstrated in theory that lattice contraction in face-centered cubic crystals is linked to their size. A size-strain relationship has already been reported in nano-ZnS $(1.5-4 \text{ nm})^{23}$ and in analogous systems such as nano-CdSe (2.3-3.7 nm). Strain-

Received: July 21, 2022 Revised: November 2, 2022 Accepted: November 2, 2022 Published: November 17, 2022





induced lattice contraction is caused by structural stress (the strength applied at the surface of the particle as a result of size reduction) and can have significant effects on the reactivity of metallic particles. $^{25-27}$

Strain has been shown to be affected by surface chemistry and, in particular, by the strength of surface-ligand interactions.²⁸ It is thus particularly important to take such interactions into consideration in complex environmental matrices when studying the environmental fate of nano-ZnS. Interactions between nano-ZnS and the organic matter have been observed in situ, for example, in biofilms. 3,4,29 In addition, laboratory studies highlighted the key properties of the organic matter that affect the aggregation state of nano-ZnS.^{29–33} To give an example, when present in solution during the first hours following nano-ZnS precipitation, organic molecules, including glutamic acid, glycine, glutathione, and cysteine, have been shown to stabilize nano-ZnS by limiting aggregation. 31-33 Finally, surface-ligand interactions involving organic molecules such as histidine, glutathione, and cysteine have been used to control the size of nano-ZnS photocatalysts.^{34–37} Although several authors reported the noticeable effects of surface interactions on nano-ZnS structural properties (mostly size) and aggregation behavior, to the best of our knowledge, to date, no systematic study has investigated the effect of surface interactions with a variety of environmentally relevant organic molecules on both particle size and strain.

The aim of this study was thus to examine the size-dependent structural strain of nano-ZnS synthesized in the presence of organic molecules. For this end, nano-ZnS in the presence of serine, cysteine, glutathione, histidine, and acetate were used to test how different surface interactions impacted the size and strain. The molecules were chosen specifically to evaluate the effects of the type of the functional group (carboxyl, thiol, hydroxyl, methyl, and imidazole), steric hindrance, organic-to-metal(Zn) ratio, and the effects of adding organic matter during or after nano-ZnS synthesis.

2. MATERIALS AND METHODS

2.1. Nano-ZnS Synthesis. A series of nano-ZnS samples were synthesized in the presence of different organic molecules (OM) including L-serine (99% purity, Acros Organics), Lcysteine (>98% purity, VWR), reduced L-glutathione (>98% purity, VWR), L-histidine (>99% purity, Sigma-Aldrich), and sodium acetate (>99% purity, Sigma-Aldrich). The resulting nano-ZnS are hereafter referred to as ZnS_ser, ZnS_cys, ZnS_GSH, ZnS_hist, and ZnS_ace, respectively. To include organic molecules, the synthesis method was adapted from bare nano-ZnS synthesis methods (see Supporting Information part I for more details). 5,7,9,28 To be representative of environmental conditions, we chose contents with excess S and organic molecules compared to Zn (a S/Zn molar ratio of 1.2 and an OM/Zn molar ratio of 2), neutral pH (7), and room temperature (~25 °C). The final concentration of ZnS was set at 0.01 M. The samples were prepared in an anoxic glovebox (N2 atmosphere) using N2-purged ultrapure water. To prevent variations in pH during synthesis due to the potential dissociation of the different protonated groups present in the organic molecules, the syntheses were performed with 0.07 M HEPES buffer (>99.5% purity, Sigma-Aldrich) to obtain a final pH of 7. Briefly, OM and Na₂S were dissolved in separated HEPES buffer solutions, and ZnCl₂ was dissolved in ultrapure water. The OM solution was mixed with the Zn solution and finally with the S solution. An additional series of

samples was synthesized with increasing concentrations of cysteine (ZnS_Cys/Zn_0.2, ZnS_Cys/Zn_0.5, and ZnS_Cys/Zn_1 for Cys/Zn molar ratios of 0.2, 0.5, and 1). Because of the lower concentration of cysteine compared to the previous set of syntheses, the concentration of HEPES was reduced to 0.035 M. For both series of samples, a nano-ZnS with no organic molecules was synthesized in the same conditions, referred to hereafter as "control A" and "control B". The parameters are summarized in Table S2.

All the sample nano-ZnS suspensions were aged for 30 h at room temperature in the dark under constant stirring in glass vials that were sealed in the anoxic glovebox. The samples were then dialyzed against ultrapure water (MWCO of 1 kDa) to remove excess salts. The nano-ZnS suspensions were then freeze-dried and the recovered solids ground to a fine powder using a mortar and pestle under an anoxic atmosphere for further characterization.

Finally, the effect of adding cysteine after nano-ZnS formation was tested on a bare nano-ZnS (bare_ZnS_S/Zn_0.5, synthesis described in Supporting Information part I) with a Cys/Zn molar ratio of 0.2. The resulting suspension was analyzed after preparation by total X-ray scattering.

2.2. Total X-ray Scattering. Synchrotron total scattering measurements were performed on beamline 11-ID-B of the Advanced Photon Source at the Argonne National Laboratory (Argonne, IL USA). All the synthesized nano-ZnS samples were measured as dry powders loaded in 1 mm O.D. Kapton capillaries. In addition, the bare nano-ZnS (bare_ZnS_S/Zn_0.5) was characterized immediately after the addition of deionized water or cysteine solution (a cysteine/Zn molar ratio of 0.2) directly in the capillary. Total scattering intensities were recorded using an amorphous silicon-based area detector (2048 × 2048 pixel, PerkinElmer). Total X-ray scattering signals were obtained with an energy of 86.7 keV [λ = 0.143 Å, monochromator Si(422)], and the distance between the sample and the detector was 16 cm. A CeO₂ crystalline reference was used for calibration (Figure S2).

Data were optimized using standard methods, 40 Fit2D software⁴¹ was used for 2D scattering images, and PDFgetX3 software⁴² was used for data correction. The background was removed using the scattering pattern of an empty polyimide capillary. A q-range from 1.4 to 24.4 Å^{-1} was used to obtain the PDF from the Fourier transform of the reduced structure factor. The structural model for sphalerite (ZnS) was used to refine the PDF using PDFgui software. 43 The following parameters were refined: scale factor, lattice parameters (a = b = c), anisotropic displacement parameters (constrained to be the same value for Zn and S), particle diameter, correlated atomic motion factor, and Q broad (peak broadening due to instrumental Q resolution). To avoid correlations between parameters, the Q broad and the anisotropic atomic motion factor were never allowed to vary together. Lattice contraction (%), that is, structural strain, is defined as $(a_{\rm nano}-a_{\rm bulk})/a_{\rm nano}$ (referred to hereafter as $\Delta a/a$), where a_{nano} is the refined lattice parameter for a nano-ZnS sample and a_{bulk} is the lattice parameter for bulk ZnS (5.4093 Å).4

The weighted residual factor $R_{\rm w}$ of the refinement is calculated as follows:

$$R_{W} = \sqrt{\frac{\sum_{i=1}^{N} w(r_{i}) [G_{\text{obs}}(r_{i}) - G_{\text{calc}}(r_{i})]^{2}}{\sum_{i=1}^{N} w(r_{i}) G_{\text{obs}}^{2}(r_{i})}}$$

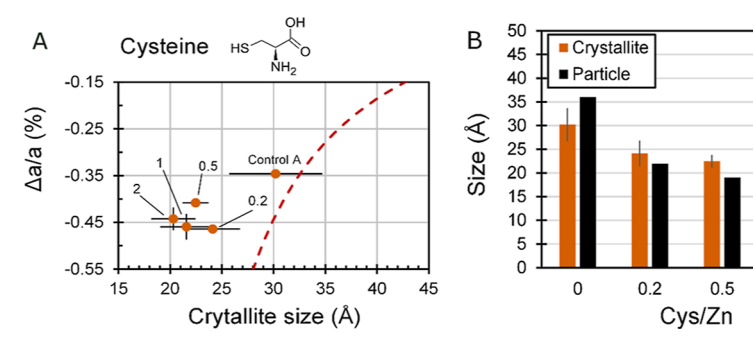


Figure 1. (A) Size—strain relationship of nano-ZnS formed in the presence of cysteine (ZnS_Cys/Zn_0.2, ZnS_Cys/Zn_0.5, ZnS_Cys/Zn_1, and ZnS_cys synthesized at a Cys/Zn molar ratio of 0.2, 0.5, 1, and 2, respectively) and a control nano-ZnS synthesized in the same conditions but with no OM (control A). The Cys/Zn molar ratio is given for each dot in (A). Crystallite sizes and strain were obtained from PDF refinement (see Materials and Methods, Section 2.2); the red dashed line corresponds to the fit of the bare nano-ZnS set of particles shown for the sake of comparison (described in Supporting Information, part I); (B) crystallite and particle sizes obtained by PDF and SAXS refinements, respectively, depending on Cys/Zn. The values and error bars are averages and standard deviation of the four values obtained from four different fits of the experimental PDF function of one particle.

where $w(r_i)$ is a multiplying factor, $G_{\rm obs}(r)$ the experimental PDF function, and $G_{\rm calc}(r)$ the refined PDF function. To estimate the uncertainty on each refined structural parameter, additional fits were performed with different initial values used for the refined parameters (scale factor, lattice parameters, anisotropic displacement parameters, particle diameter, correlated atomic motion factor, and Q broad). Four fits were selected according to two criteria: (i) the values of the refined parameters were physically consistent and (ii) the quality of the fit was acceptable (i.e., all PDF peaks considered by refinement and $R_{\rm w} < 0.3$). The values presented in this study (size, lattice parameter) are the average of the four values obtained with the four fits, and the error bars represent the standard deviation for the same four values.

2.3. Small-Angle X-ray Scattering. Small-angle X-ray scattering (SAXS) experiments were performed on nano-ZnS powders placed inside a 1 mm Kapton capillary using a laboratory SAXS beamline (Xeuss 2.0) equipped with a copper microfocus X-ray source. The counting time was 1 h for each measurement. The scattering image was recorded on a direct photon counting 1 M pixels Pilatus camera protected from the direct X-ray beam by a 3 mm beamstop. The SAXS profiles of intensity [I(q)] versus scattering vectors (q) were obtained by radial averaging of the scattered X-ray 2D images as a function of q, where $q = 4\pi \sin \theta/\lambda$ (λ and 2θ denote the incident wavelength and the scattering angle, respectively). The scattering angles were calibrated using a silver behenate lamellar-like phase that has a well-known d_{001} repeat distance of 5.838 nm, thus enabling precise measurement of the distance between the sample and the detector. The radial averaged SAXS profiles were further corrected for the scattering contribution of the empty Kapton capillary and the electronic background using pySAXS software (https:// pypi.org/project/pySAXS/). The scattering profiles obtained were typical of powders made of aggregated spheres. The increase in intensity at the lowest angles observed for the cysteine-containing sample originated from interparticle scattering and are not discussed in the present work. We estimated the nano-ZnS particle size for each powder using the fit of the intermediate q range of the scattering curve obtained by a monodisperse sphere model.

2.4. Statistics. The Scikit-posthocs Python package was used for statistical analysis to compare sizes and lattice contraction values. ⁴⁵ A Kruskal–Wallis test was used to

compare all the samples (n=21) according to one parameter (size or lattice contraction). The four values obtained from the four different PDF refinements were used for this comparison. In cases of rejection of the null hypothesis (H_0 = all samples are from the same population), a Conover posthoc test was used for multiple pairwise comparison with a step-down method using Bonferroni adjustments. Differences were considered significant for an adjusted p-value < 0.05.

3. RESULTS AND DISCUSSION

Environmentally relevant organic molecules with functional groups of varying affinity for Zn (-OH, -COOH, -NH₂, -SH, imidazole) were used to investigate the role of these interactions in the size and strain of nano-ZnS. In the following, the structural properties of nano-ZnS synthesized in the presence of organic molecules are compared with (i) a control nano-ZnS synthesized in the same conditions with no organic molecules and with (ii) the set of bare nano-ZnS represented by the quadratic function for which synthetic conditions were varied to obtain nano-ZnS of different sizes. The size-strain relationship obtained for bare nano-ZnS is presented in Supporting Information, part I. As expected based on previous literature data, this relationship can be modeled using a quadratic function. ²²

3.1. Effect of Thiol Groups on Size and Strain. Cysteine was used to assess the impact of thiol groups, which are known to have a strong affinity for ZnS surfaces. ⁴⁶ In addition, cysteine has the highest stability constant with zinc (log K = 9.11) ⁴⁷ compared with other amino acids.

Nano-ZnS was synthesized using an increasing Cys/Zn ratio from 0.2 to 2 and compared to a control synthesized with no cysteine (control A). The size—strain relationship is shown in Figure 1A.

The nano-ZnS synthesized in the presence of cysteine exhibited both smaller average crystallite domains and higher strain than the control nano-ZnS. The decrease in the size of the crystallite domain was accompanied by a decrease in particle size, as revealed by SAXS (Figure 1B). In addition, for each particle, the sizes of the crystallite domain and of the particle were found to be identical within the range of the refinement error (Figure 1B), strongly suggesting that the particles formed were made of a single crystal (i.e., monocrystalline) and did not have a highly disordered surface layer and/or internal disorder.

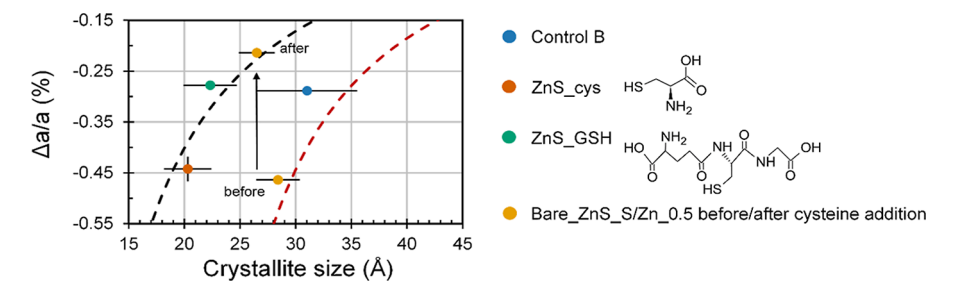


Figure 2. Sizes and strains of nano-ZnS formed in the presence of cysteine, glutathione (ZnS_cys and ZnS_GSH), a control nano-ZnS synthesized in the same conditions but with no OM (control B) and the bare nano-ZnS before and after exposure to cysteine (bare_ZnS_S/Zn_0.5 and bare_ZnS_S/Zn_0.5_cys) obtained from PDF refinement (see Materials and Methods, Section 2.2). The red and black dashed lines correspond to the quadratic function that fits the size—strain relationship of the bare nano-ZnS set of particles (Supporting Information, part I) and nano-ZnS particles formed in the presence of the thiol functional group (i.e., ZnS_cys, ZnS_GSH, bare_ZnS_S/Zn_0.5_cys), respectively. The values and error bars are averages and standard deviations of the four values obtained from four different fits of the experimental PDF function of one particle.

Interestingly, when cysteine was added in the system at the beginning of the synthesis, the size—strain properties of the synthesized nano-ZnS did not vary as a function of the Cys/Zn ratio in the range 0.2–2. At the lowest Cys/Zn ratio (ZnS_Cys/Zn_0.2), the estimated coverage of the surface of the nano-ZnS by cysteine molecules was 40% (Table S4) which seems sufficient to inhibit particle growth in the same way as when cysteine was added in excess (ZnS_cys with a Cys/Zn ratio of 2).

The surface density of thiol—surface interactions depends not only on the thiol-Zn ratio but also on the size of the thiol molecule (steric hindrance), which may also affect the size—strain properties of the nano-ZnS formed. In particular, if we consider environmental conditions, thiol molecules can often be bigger than cysteine molecules. The biomolecule glutathione (GSH) was chosen to investigate the effect of the size of the organic molecules because it exhibits a thiol and other functional groups that are similar to cysteine but is significantly larger than cysteine (307.3 vs 121.2 g mol⁻¹).

Nano-ZnS formed in the presence of GSH at a GSH/Zn ratio of 2 was found to be slightly bigger than nano-ZnS formed in the presence of cysteine (22 and 20 Å, for ZnS_GSH and ZnS_cys, respectively, for an OM/Zn ratio of 2, Figure 2) but based on our reported refinement errors, the difference was not significant. However, ZnS GSH exhibited a lattice contraction of -0.28%, significantly lower than ZnS cys (-0.44%). Taken together, these two observations suggest that the presence of GSH during synthesis influenced nano-ZnS growth but that the effects were less marked than with cysteine. Indeed, the higher steric hindrance for GSH could limit the number of thiol groups on the surface of nano-ZnS, compared with that for cysteine. The lesser strain observed with GSH than with cysteine was in line with the size-strain relationship observed for bare nano-ZnS, which showed a decrease in strain with bigger crystallite sizes (see Supporting Information, part I).

The results described above were obtained with thiol-bearing molecules that were added during the synthesis of nano-ZnS and that affected both the degree of particle growth and structural strain. To study the effect of thiol functional groups on lattice contraction independently of its effect on size, the samples of as-prepared bare nano-ZnS (bare_ZnS_S/Zn_0.5, with a size of 28 Å and a lattice contraction of -0.46%, synthesized using the bare nano-ZnS method, Supporting Information part I) were mixed with cysteine. This bare nano-ZnS sample was chosen because of its small

size and high strain. In Figure 2, the dot corresponding to the bare nano-ZnS before the addition of cysteine (bare ZnS S/ Zn_0.5) fits on the red dashed line representing the bare nano-ZnS set (described in Figure S6). As shown by the two yellow dots in Figure 2, adding cysteine after nano-ZnS synthesis did not significantly alter the size of the nano-ZnS (27 Å); however, lattice contraction dropped to -0.21%. This suggests that binding functional groups (e.g., thiol) strongly to the surface reduces nano-ZnS internal strain and that this effect is independent of particle size. This strain release could be due to a similar mechanism to that reported by Zhang et al. (2003), 48 that is, a decrease in internal energy and an increase in crystallinity induced by the interaction between water and the surface of ZnS. However, additional observations with thiols added after the synthesis are needed to conclude on a systematic strain release.

The size—strain relationship of the cysteine-coated nano-ZnS formed in two steps (bare_ZnS_S/Zn_0.5_cys) is in line with the nano-ZnS formed directly in the presence of cysteine or GSH (ZnS_cys and ZnS_GSH). In contrast, the nano-ZnS synthesized with no organic molecules (control B and bare_ZnS_S/Zn_0.5) are in line with the bare nano-ZnS size—strain relationship (red dashed line). Interestingly, as shown in Figure 2, the presence of thiol groups caused the size—strain relationship to shift to an approximately 1 nm size smaller than the one of bare nano-ZnS. Indeed, the black dashed line in Figure 2 corresponds to the red dashed line (bare nano-ZnS size—strain relationship, Figure S6) offset by 1 nm. This suggests that thiol-bearing molecules lead to the formation of smaller nano-ZnS when present before ZnS precipitation.

3.2. Organic Molecules with No Effects or Only Slight Effects on the Particle Size and Strain. To check if the cysteine and GSH effects on nano-ZnS structural properties were due to the affinity of thiol for the surface of ZnS, a set of nano-ZnS were synthesized in the presence of organic molecules that are known to have lower affinities for the ZnS surface than thiol groups. Serine and histidine were chosen to study the effect of hydroxyl and imidazole functional groups compared with the effect of the thiol functional group present in cysteine. Indeed, these three molecules have a similar composition (—COOH and —NH₂ groups) except for the third functional group that varies (—SH, —OH, and—imidazole groups, Figure 3). Acetate was chosen to investigate the effect of the carboxyl functional group (—COOH) alone.

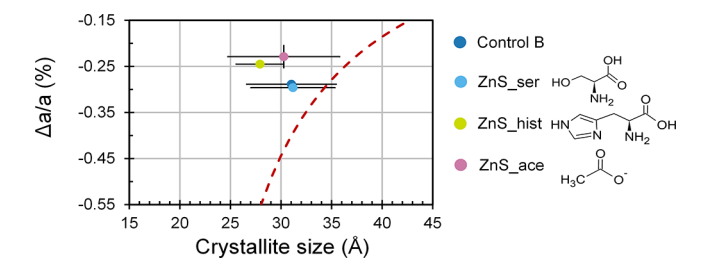


Figure 3. Sizes and strains of nano-ZnS formed in the presence of serine, histidine, acetate (ZnS_ser, ZnS_hist, and ZnS_ace, respectively); a control nano-ZnS synthesized in the same conditions but with no OM (control B), obtained from PDF refinement (see Materials and Methods, Section 2.2). The red dashed line corresponds to the fit of the bare nano-ZnS set of particles (Supporting Information, part I) shown for the sake of comparison. The values and error bars are averages and standard deviations of the four values obtained from four different fits for the experimental PDF function of one particle.

The size and strain values of ZnS_ser, ZnS_hist, and ZnS_ace, the nano-ZnS synthesized in the presence of serine, histidine, acetate (OM/Zn ratio of 2), and the corresponding control nano-ZnS synthesized in the same conditions but with no OM are presented in Figure 3 and Supporting Information part II.

No significant effect on crystallite domain size was observed for nano-ZnS formed in the presence of serine, acetate, and histidine (within the range of refinement error). This can be explained by the fact that the surface interactions of the organic molecules and nano-ZnS were not strong enough to impact particle growth.

However, the presence of histidine and acetate reduced the amount of strain of the as-formed nano-ZnS (-0.25 and -0.23% for ZnS hist and ZnS ace compared to -0.29 and -0.30% for the control nano-ZnS and ZnS ser). Molecular dynamics simulations were used to calculate binding energies between the surface of ZnS and various organic molecules and showed that most molecules including serine, acetate, and histidine bind poorly to the surface of ZnS. 46 The histidine binding energy (3.06 kJ/mol) is slightly higher than that for serine (1.95 kJ/mol). This suggests that the imidazole group of histidine has a slightly higher affinity for the nano-ZnS surface than for the hydroxide functional group of serine, 46 which could explain the slight decrease in strain. For acetate, the interaction mechanism is not clear [not considered in Nawrocki and Cieplak (2014)]⁴⁶ but may originate from the hydrophobicity of the -CH₃ group in addition to potential surface affinity. Indeed, the ZnS surface is mostly hydrophobic, 46 and the hydrophobic -CH₃ extremity of acetate has been shown to initiate interactions on other hydrophobic surfaces including gold.⁴⁹

Nano-ZnS synthesized with serine (ZnS_ser) exhibited similar crystallite domain size and strain to those of the control nano-ZnS. This suggests that serine and its functional groups, –COOH, –OH, and –NH₂, have no effects on the crystallite domain size and strain of nano-ZnS. As the thiol group was the only group that differed between cysteine and serine, we conclude that the interaction between the thiol group of cysteine and the nano-ZnS surface was responsible for affecting nano-ZnS structural properties. This conclusion is supported by molecular dynamics simulations that showed a binding energy of 98 kJ/mol for cysteine on the ZnS (110) surface,

which is 1 to 2 orders of magnitude higher than those for histidine and serine. 46 Such a difference can be explained by the formation of a covalent disulfide bond for cysteine at the ZnS surface. 46

Based on nucleation and growth principles,⁵⁰ the thiol binding with Zn or S surface atoms during nano-ZnS formation could inhibit the growth by blocking growth sites and consequently favor the formation of smaller nano-ZnS compared to the cysteine-free system. Also, if the surface energy decreases as a consequence of thiol binding, the system is thermodynamically more favorable for smaller crystal sizes (reduced critical nucleus size) than a cysteine-free system.

3.3. Environmental Implications. Our results support the results obtained by Zhang et al. (2003), ⁴⁸ showing that the composition of the medium determines the structure of nanoparticles through surface interactions. Here, we specifically investigated the role of different organic functional groups in nano-ZnS size and strain. These results also represent a step forward in understanding the formation of other analogous metallic nanoparticles and their fate in the environment. Indeed, nano-ZnS can be a model nanoparticle for several other sulfide metallic particles with a cubic structure that are formed in anoxic environments or manufactured (e.g., HgS, CdS).

There is also a critical need to understand the specific formation of nano-ZnS in the environment. One of the biggest pools of nano-ZnS formation is Zn-rich organic waste (OW)¹⁰ as nano-ZnS are systematically formed either during the storage of liquid OW or during the anaerobic digestion of solid and liquid OW. Our results revealed the key role of thiolcontaining molecules in nano-ZnS formation. The organic composition of OW is continuously changing as the organic matter is broken down into progressively smaller molecules during the process of digestion. 51 Thiols are one of the main species of sulfur involved in these systems. 52 Therefore, thiols are expected to interact with nano-ZnS either during or after their formation. For example, if they are present during nano-ZnS formation, the thiolated molecules in OW could be a factor explaining the small size of nano-ZnS in OW5,6 or in other organic-rich matrices such as biofilms.4

The mechanisms controlling the fate of these small nano-ZnS also need further investigation. Indeed, small nano-ZnS (3-5 nm) were seen to undergo transformation in soil much faster (within months)^{5,9} than their 25–40 nm homologues (within years).⁵³ The size threshold below which new properties of the nanomaterial are observed is typically 20-30 nm. 54 These specific nanoscale properties could be related to size-dependent properties such as lattice contraction, thermal properties, or interfacial reactivity.⁵⁴ More specifically, Huang et al. (2007)⁵⁵ showed that the effect of size on lattice contraction was significant only in the case of metallic nanoparticles less than 5 nm in size. Consequently, we hypothesize that such a size-strain relationship in nano-ZnS smaller than 5 nm could explain the difference in reactivity between them and their 25-40 nm homologues. Beyond intrinsic nano-ZnS properties (size, strain, and organic coating), extrinsic properties (medium composition, e.g., soil properties) also influence the fate of nano-ZnS. For example, we recently showed that the dissolution kinetics of nano-ZnS applied on soil and the availability of released ions (Zn2+) were controlled by the soil properties (e.g., mineralogy and texture). However, we still need to see if, in such complex environments, that is, amended soils, the effect of intrinsic

properties plays a more important role in the transformation of these incidental nano-ZnS than extrinsic properties.

ASSOCIATED CONTENT

Solution Supporting Information

The Supporting Information is available free of charge at https://pubs.acs.org/doi/10.1021/acs.est.2c05268.

Size-strain relationship for the bare nano-ZnS set, experimental data for the nano-ZnS synthesized with organic molecules (pair distribution function, SAXS), and surface coverage estimation (PDF)

AUTHOR INFORMATION

Corresponding Author

Maureen Le Bars — Aix Marseille Univ, CNRS, IRD, INRAE, Coll France, CEREGE, Aix-en-Provence 13545, France; UPR Recyclage et Risque, CIRAD, Montpellier, France; Recyclage et Risque, Univ. Montpellier, CIRAD, Montpellier F-34398, France; Present Address: Institute of Biogeochemistry & Pollutant Dynamics, ETH Zurich, Universitätstrasse 16, 8092 Zurich, Switzerland; orcid.org/0000-0003-4149-4951; Email: maureen.lebars@usys.ethz.ch

Authors

Clément Levard — Aix Marseille Univ, CNRS, IRD, INRAE, Coll France, CEREGE, Aix-en-Provence 13545, France;
orcid.org/0000-0001-7507-7959

Samuel Legros — UPR Recyclage et Risque, CIRAD, Montpellier, France; Recyclage et Risque, Univ. Montpellier, CIRAD, Montpellier F-34398, France; orcid.org/0000-0001-7081-6679

Vladimir Vidal – Aix Marseille Univ, CNRS, IRD, INRAE, Coll France, CEREGE, Aix-en-Provence 13545, France

Alejandro Fernandez-Martinez — Univ. Grenoble Alpes, Univ. Savoie Mont Blanc, CNRS, IRD, IFSTTAR, ISTerre, Grenoble 38000, France; orcid.org/0000-0001-5073-9629

F. Marc Michel – Department of Geosciences, Virginia Polytechnic Institute and State University, Blacksburg, Virginia 24061, United States

Antoine Thill – NIMBE, UMR 3685 CEA, CNRS, Université Paris-Saclay, CEA Saclay, Gif-sur-Yvette Cedex 91191, France; orcid.org/0000-0003-0163-3638

Benedicte Prelot — ICGM, Univ Montpellier, CNRS, ENSCM, Montpellier 34290, France; orcid.org/0000-0002-9478-6694

Gabrielle Dublet-Adli – Norwegian Geotechnical Institute, Oslo 0806, Norway

Daniel Borschneck – Aix Marseille Univ, CNRS, IRD, INRAE, Coll France, CEREGE, Aix-en-Provence 13545, France

Jérôme Rose — Aix Marseille Univ, CNRS, IRD, INRAE, Coll France, CEREGE, Aix-en-Provence 13545, France;
orcid.org/0000-0003-3071-8147

Emmanuel Doelsch – UPR Recyclage et Risque, CIRAD, Montpellier, France; Recyclage et Risque, Univ. Montpellier, CIRAD, Montpellier F-34398, France

Complete contact information is available at: https://pubs.acs.org/10.1021/acs.est.2c05268

Notes

The authors declare no competing financial interest.

ACKNOWLEDGMENTS

We are grateful to the French Environment and Energy Management Agency (ADEME) and the French Agricultural Research Centre for International Development (CIRAD) for funding the PhD scholarship of M.L.B. This study was part of the DIGESTATE project, funded by the French National Research Agency (ANR) under grant ANR-15-CE34-0003-01. We acknowledge Advanced Photon Source (APS) for access to synchrotron radiation facilities, and we would like to thank Olaf J. Borkiewicz for assistance in using the 11-ID-B beamline. F.M.M. acknowledges support from the National Science Foundation (NSF) through CAREER-1652237 and the Virginia Tech Center for Earth and Environmental Nanotechnology "NanoEarth" (NNCI-1542100).

REFERENCES

- (1) Fang, X. S.; Zhai, T. Y.; Gautam, U. K.; Li, L.; Wu, L. M.; Yoshio, B.; Golberg, D. ZnS nanostructures: From synthesis to applications. *Prog. Mater. Sci.* **2011**, *56*, 175–287.
- (2) Lee, G. J.; Wu, J. J. Recent developments in ZnS photocatalysts from synthesis to photocatalytic applications A review. *Powder Technol.* **2017**, 318, 8–22.
- (3) Labrenz, M.; Druschel, G. K.; Thomsen-Ebert, T.; Gilbert, B.; Welch, S. A.; Kemner, K. M.; Logan, G. A.; Summons, R. E.; Stasio, G.; Bond, P. L.; Lai, B.; Kelly, S. D.; Banfield, J. F. Formation of sphalerite (ZnS) deposits in natural biofilms of sulfate-reducing bacteria. *Science* **2000**, *290*, 1744–1747.
- (4) Moreau, J. W.; Webb, R. I.; Banfield, J. F. Ultrastructure, aggregation-state, and crystal growth of biogenic nanocrystalline sphalerite and wurtzite. *Am. Mineral.* **2004**, *89*, 950–960.
- (5) Formentini, T. A.; Legros, S.; Fernandes, C. V. S.; Pinheiro, A.; Le Bars, M.; Levard, C.; Mallmann, F. J. K.; da Veiga, M.; Doelsch, E. Radical change of Zn speciation in pig slurry amended soil: Key role of nano-sized sulfide particles. *Environ. Pollut.* **2017**, 222, 495–503.
- (6) Kim, B.; Levard, C.; Murayama, M.; Brown, G. E.; Hochella, M. F. Integrated Approaches of X-Ray Absorption Spectroscopic and Electron Microscopic Techniques on Zinc Speciation and Characterization in a Final Sewage Sludge Product. *J. Environ. Qual.* **2014**, *43*, 908–916.
- (7) Le Bars, M.; Legros, S.; Levard, C.; Chaurand, P.; Tella, M.; Rovezzi, M.; Browne, P.; Rose, J.; Doelsch, E. Drastic Change in Zinc Speciation during Anaerobic Digestion and Composting: Instability of Nanosized Zinc Sulfide. *Environ. Sci. Technol.* **2018**, *52*, 12987–12996
- (8) Legros, S.; Levard, C.; Marcato-Romain, C. E.; Guiresse, M.; Doelsch, E. Anaerobic Digestion Alters Copper and Zinc Speciation. *Environ. Sci. Technol.* **2017**, *51*, 10326–10334.
- (9) Le Bars, M.; Legros, S.; Levard, C.; Chevassus-Rosset, C.; Montes, M.; Tella, M.; Borschneck, D.; Guihou, A.; Angeletti, B.; Doelsch, E. Contrasted fate of zinc sulfide nanoparticles in soil revealed by a combination of X-ray absorption spectroscopy, diffusive gradient in thin films and isotope tracing. *Environ. Pollut.* **2022**, 292, 118414.
- (10) Levard, C.; Le Bars, M.; Formentini, T.; Legros, S.; Doelsch, E. Organic waste-borne ZnS nanoparticles: The forgotten ones. *Environ. Pollut.* **2022**, 308, 119629.
- (11) Hawkesford, M.; Horst, W.; Kichey, T.; Lambers, H.; Schjoerring, J.; White, I. S.; White, P.; Functions of Macronutrients. In *Marschner's Mineral Nutrition of Higher Plants*, 3rd ed; Marschner, P., Ed.; Elseiver, 2012; Chapter 6, pp 135–189.
- (12) Lewis, A. E. Review of metal sulphide precipitation. *Hydrometallurgy* **2010**, *104*, 222–234.
- (13) Andreini, C.; Banci, L.; Bertini, I.; Rosato, A. Counting the zinc-proteins encoded in the human genome. *J. Proteome Res.* **2006**, *5*, 196–201.
- (14) Broadley, M.; Brown, P.; Cakmak, I.; Zhao, Z.; Zhao, F. J.Function of Nutrients: Micronutrients. In Marschner's Mineral

- Nutrition of Higher Plants, 3rd ed; Marschner, P., Ed.; Elseiver, 2012; Chapter 7, pp 191-248.
- (15) Alloway, B. J. Soil factors associated with zinc deficiency in crops and humans. *Environ. Geochem. Health* **2009**, *31*, 537–548.
- (16) Lowe, N. M. The global challenge of hidden hunger: perspectives from the field. *Proc. Nutr. Soc.* **2021**, *80*, 283–289.
- (17) Joy, E. J. M.; Ander, E. L.; Young, S. D.; Black, C. R.; Watts, M. J.; Chilimba, A. D. C.; Chilima, B.; Siyame, E. W. P.; Kalimbira, A. A.; Hurst, R.; Fairweather-Tait, S. J.; Stein, A. J.; Gibson, R. S.; White, P. J.; Broadley, M. R. Dietary mineral supplies in Africa. *Physiol. Plantarum* **2014**, *151*, 208–229.
- (18) Chaudri, A. M.; Allain, C. M. G.; Barbosa-Jefferson, V. L.; Nicholson, F. A.; Chambers, B. J.; McGrath, S. P. A study of the impacts of Zn and Cu on two rhizobial species in soils of a long-term field experiment. *Plant Soil* **2000**, *221*, 167–179.
- (19) Broadley, M. R.; White, P. J.; Hammond, J. P.; Zelko, I.; Lux, A. Zinc in plants. *New Phytol.* **2007**, *173*, 677–702.
- (20) Zhang, H. Z.; Chen, B.; Banfield, J. F. Particle Size and pH Effects on Nanoparticle Dissolution. *J. Phys. Chem. C* **2010**, *114*, 14876–14884.
- (21) Gilbert, B.; Huang, F.; Zhang, H. Z.; Waychunas, G. A.; Banfield, J. F. Nanoparticles: Strained and stiff. *Science* **2004**, *305*, 651–654.
- (22) Jiang, Q.; Liang, L. H.; Zhao, D. S. Lattice contraction and surface stress of fcc nanocrystals. *J. Phys. Chem. B* **2001**, *105*, 6275–6277
- (23) Lu, S. H.; Chen, T. F.; Wang, A. J.; Wu, Z. L.; Wang, Y. S. Lattice and optical property evolution of ultra-small ZnS quantum dots grown from a single-source precursor. *Appl. Surf. Sci.* **2014**, *299*, 116–122.
- (24) Masadeh, A. S.; Božin, E. S.; Farrow, C. L.; Paglia, G.; Juhas, P.; Billinge, S. J. L.; Karkamkar, A.; Kanatzidis, M. G. Quantitative size-dependent structure and strain determination of CdSe nanoparticles using atomic pair distribution function analysis. *Phys. Rev. B* **2007**, *76*, 115413.
- (25) Mavrikakis, M.; Hammer, B.; Nørskov, J. K. Effect of Strain on the Reactivity of Metal Surfaces. *Phys. Rev. Lett.* **1998**, *81*, 2819–2822.
- (26) Strasser, P.; Koh, S.; Anniyev, T.; Greeley, J.; More, K.; Yu, C. F.; Liu, Z. C.; Kaya, S.; Nordlund, D.; Ogasawara, H.; Toney, M. F.; Nilsson, A. Lattice-strain control of the activity in dealloyed core-shell fuel cell catalysts. *Nat. Chem.* **2010**, *2*, 454–460.
- (27) Pratt, A.; Lari, L.; Hovorka, O.; Shah, A.; Woffinden, C.; Tear, S. P.; Binns, C.; Kröger, R. Enhanced oxidation of nanoparticles through strain-mediated ionic transport. *Nat. Mater.* **2014**, *13*, 26–30.
- (28) Gilbert, B.; Huang, F.; Lin, Z.; Goodell, C.; Zhang, H.; Banfield, J. F. Surface Chemistry Controls Crystallinity of ZnS Nanoparticles. *Nano Lett.* **2006**, *6*, 605–610.
- (29) Moreau, J. W.; Weber, P. K.; Martin, M. C.; Gilbert, B.; Hutcheon, I. D.; Banfield, J. F. Extracellular proteins limit the dispersal of biogenic nanoparticles. *Science* **2007**, *316*, 1600–1603.
- (30) Deonarine, A.; Lau, B. L. T.; Aiken, G. R.; Ryan, J. N.; Hsu-Kim, H. Effects of Humic Substances on Precipitation and Aggregation of Zinc Sulfide Nanoparticles. *Environ. Sci. Technol.* **2011**, *45*, 3217–3223.
- (31) Gondikas, A. P.; Jang, E. K.; Hsu-Kim, H. Influence of amino acids cysteine and serine on aggregation kinetics of zinc and mercury sulfide colloids. *J. Colloid Interface Sci.* **2010**, 347, 167–171.
- (32) Gondikas, A. P.; Masion, A.; Auffan, M.; Lau, B. L. T.; Hsu-Kim, H. Early-stage precipitation kinetics of zinc sulfide nanoclusters forming in the presence of cysteine. *Chem. Geol.* **2012**, 329, 10–17.
- (33) Lau, B. L. T.; Hsu-Kim, H. Precipitation and growth of zinc sulfide nanoparticles in the presence of thiol-containing natural organic ligands. *Environ. Sci. Technol.* **2008**, *42*, 7236–7241.
- (34) Bae, W.; Mehra, R. K. Cysteine-capped ZnS nanocrystallites: Preparation and characterization. *J. Inorg. Biochem.* **1998**, 70, 125–135
- (35) Bae, W. O.; Abdullah, R.; Henderson, D.; Mehra, R. K. Characteristics of glutathione-capped ZnS nanocrystallites. *Biochem. Biophys. Res. Commun.* 1997, 237, 16–23.

- (36) Devi, L. M.; Negi, D. P. S. Effect of starting pH and stabilizer/metal ion ratio on the photocatalytic activity of ZnS nanoparticles. *Mater. Chem. Phys.* **2013**, *141*, 797–803.
- (37) Kho, R.; Nguyen, L.; Torres-Martínez, C. L.; Mehra, R. K. Zinc-histidine as nucleation centers for growth of ZnS nanocrystals. *Biochem. Biophys. Res. Commun.* **2000**, 272, 29–35.
- (38) Chupas, P. J.; Chapman, K. W.; Lee, P. L. Applications of an amorphous silicon-based area detector for high-resolution, high-sensitivity and fast time-resolved pair distribution function measurements. *J. Appl. Crystallogr.* **2007**, *40*, 463–470.
- (39) Chupas, P. J.; Chapman, K. W.; Jennings, G.; Lee, P. L.; Grey, C. P. Watching nanoparticles grow: The mechanism and kinetics for the formation of TiO₂-supported platinum nanoparticles. *J. Am. Chem. Soc.* **2007**, *129*, 13822–13824.
- (40) Hoeher, A.; Mergelsberg, S.; Borkiewicz, O. J.; Dove, P. M.; Michel, F. M. A new method for in situ structural investigations of nano-sized amorphous and crystalline materials using mixed-flow reactors. *Acta Crystallogr., Sect. A: Found. Adv.* **2019**, *75*, 758–765.
- (41) Hammersley, A. P.; Svensson, S. O.; Hanfland, M.; Fitch, A. N.; Hausermann, D. Two-dimensional detector software: From real detector to idealised image or two-theta scan. *High Pres. Res.* **1996**, *14*, 235–248.
- (42) Juhás, P.; Davis, T.; Farrow, C. L.; Billinge, S. J. L. PDFgetX3: a rapid and highly automatable program for processing powder diffraction data into total scattering pair distribution functions. *J. Appl. Crystallogr.* **2013**, *46*, 560–566.
- (43) Farrow, C. L.; Juhas, P.; Liu, J. W.; Bryndin, D.; Bozin, E. S.; Bloch, J.; Proffen, T.; Billinge, S. J. L. PDFfit2 and PDFgui: computer programs for studying nanostructure in crystals. *J. Phys. Condens. Matter* **2007**, *19*, 335219.
- (44) Skinner, B. J. Unit-Cell Edges of Natural and Synthetic Sphalerites. *Am. Mineral.* **1961**, *46*, 1399–1411.
- (45) Terpilovskii, M. A. scikit-posthocs: Pairwise multiple comparison tests in Python. J. Open Source Software 2019, 4, 1169.
- (46) Nawrocki, G.; Cieplak, M. Interactions of aqueous amino acids and proteins with the (110) surface of ZnS in molecular dynamics simulations. *J. Chem. Phys.* **2014**, *140*, 095101.
- (47) Burgess, D. R.NIST SRD 46. Critically Selected Stability Constants of Metal Complexes: Version 8.0 for Windows; National Institute of Standards and Technology, 2004.
- (48) Zhang, H. Z.; Gilbert, B.; Huang, F.; Banfield, J. F. Waterdriven structure transformation in nanoparticles at room temperature. *Nature* **2003**, 424, 1025–1029.
- (49) Hoefling, M.; Iori, F.; Corni, S.; Gottschalk, K. E. Interaction of Amino Acids with the Au(111) Surface: Adsorption Free Energies from Molecular Dynamics Simulations. *Langmuir* **2010**, *26*, 8347–8351
- (50) De Yoreo, J. J.; Vekilov, P. G. 3. Principles of Crystal Nucleation and Growth. Rev. Mineral. Geochem. 2003, 54, 57–94.
- (51) Deublein, D.; Steinhauser, A.Biogas from Waste and Renewable Resources: An Introduction; John Wiley & Sons, 2011.
- (52) van Hullebusch, E. D.; Yekta, S. S.; Calli, B.; Fermoso, F. G.Biogeochemistry of major elements in anaerobic digesters: carbon, nitrogen, phosphorus, sulfur and iron. In *Trace Elements in Anaerobic Biotechnologies*, Fermoso, F. G., van Hullebusch, E. D., Collins, G., Roussel, J., Mucha, A. P., Esposito, G., Eds.; OAPEN Library, 2019; Chapter 1, pp 1–22.
- (53) Voegelin, A.; Jacquat, O.; Pfister, S.; Barmettler, K.; Scheinost, A. C.; Kretzschmar, R. Time-Dependent Changes of Zinc Speciation in Four Soils Contaminated with Zincite or Sphalerite. *Environ. Sci. Technol.* **2011**, *45*, 255–261.
- (54) Auffan, M.; Rose, J.; Bottero, J. Y.; Lowry, G. V.; Jolivet, J. P.; Wiesner, M. R. Towards a definition of inorganic nanoparticles from an environmental, health and safety perspective. *Nat. Nanotechnol.* **2009**, *4*, 634–641.
- (55) Huang, Z. X.; Thomson, P.; Di, S. L. Lattice contractions of a nanoparticle due to the surface tension: A model of elasticity. *J. Phys. Chem. Solids* **2007**, *68*, 530–535.